Temporal Ablation of Primary Cilia Impairs Brainwave Patterns Implicated in Memory Formation

Matthew Strobel[1,2 *], Liyan Qiu[1], Aldebaran Hofer[2], and Xuanmao Chen[1 *]

[1] Department of Molecular, Cellular, and Biomedical Sciences, College of Life Sciences and Agriculture, University of New Hampshire, Durham, NH 03824

[2] Harvard Medical School and the VA Boston Healthcare System and the Department of Surgery, Brigham and Women's Hospital, 1400 VFW Parkway, West Roxbury, MA 02132, USA.

* Correspondence should be addressed to Matthew Strobel (mstrobel@bwh.harvard.edu) or Xuanmao Chen (Xuanmao.Chen@unh.edu)

Key Words: Primary Cilia, EEG/EMG, Sleep Analysis, Cross-frequency coupling (CFC), Phase-Amplitude Coupling, Memory.

Author Contributions: XC and MS designed research; MS and LQ performed the research; MS analyzed the data; XC and AH provided resources; MS wrote the manuscript, and XC and AH revised it.

Conflict of Interest Statement: The authors declare that the research was conducted in the absence of any commercial or financial conflicts of interest.

Acknowledgements: This study was supported by NIH Grants K01AG054729, P20GM113131, R15MH126317, R15MH125305, COLE Neuroscience Research Awards, and UNH CoRE PRP awards to XC. MS was supported by a Summer TA Research Fellowship (STAF) of UNH Graduate School.

Abstract

The primary cilium is a hair-like organelle that hosts molecular machinery for various developmental and homeostatic signaling pathways. Its alteration can cause severe ciliopathies such as the Bardet-Biedl and Joubert syndromes, but is also linked to Alzheimer's disease, clinical depression, and autism spectrum disorder. These afflictions are caused by disturbances in a variety of genes but a common phenotype amongst them is cognitive impairment. Cilia-mediated neural function has generally been examined in relation to these diseases or other developmental defects, but the role of cilia in brain function and memory consolidation is unknown. To elucidate the role of cilia in neural activity and cognitive function, we temporally ablated primary cilia in adult mice before performing electroencephalogram/electromyogram (EEG/EMG) recordings. We found that cilia deficient mice had altered sleep architecture, reduced EEG power, and attenuated phase-amplitude coupling, a process that underlies memory consolidation. These results highlight the growing significance of cilia, demonstrating that they are not only necessary in early neurodevelopment, but also regulate advanced neural functions in the adult brain.

Introduction

Primary cilia are specialized organelles that emanate from the plasma membrane of vertebrate cells. Despite being contiguous with the cellular membrane, the ciliary membrane maintains a distinct lipid and protein composition [1], [2]. The cilium also has a filter-like transition zone at the basal end which requires chaperoning and an intraflagellar transport system to traverse for proteins with a stokes radii > 8nm [3], [4]. This membrane composition and barrier to diffusion isolates the cilium from the cell body and allows it to operate as a unique microdomain.

Numerous intracellular signaling pathways have been linked to primary cilia including Sonic Hedgehog (Shh), WNT, Notch, HIPPO, PDGF, mTOR, and G-protein coupled receptors (GPCRs)-mediated cAMP pathways. Primary cilia therefore regulate many key developmental, sensory, and homeostatic pathways. [1], [5]–[7]. Mutations to genes in these pathways or other ciliary genes can lead to severe developmental disorders known as ciliopathies. To date over 60 ciliary genes have been found to impair neurological development leading to conditions such as Joubert, Meckel, and Bardet-Biedl syndromes (BBS) [8]. Outside of these classically identified ciliopathies, ciliary genes have also been connected to numerous other neurological conditions. The autism spectrum disorder genes FXS and AHI1 have been linked through genome-wide association studies to Joubert Syndrome and are believed to act as signal transducers of Shh. Disruption of these genes leads to reduced neuronal differentiation, dendritic complexity, memory deficits, and reduced ciliation of neurons in the hippocampal dentate gyrus [9]–[12]. In Alzheimer's disease (AD) the ciliary receptors $p75^{NTR}$, SSTR3, and 5HTR6 have been implicated in the progression of cognitive decline. It has been shown that $p75^{NTR}$ can be aberrantly activated by amyloid-beta (Aβ) peptides resulting in tyrosine kinase mediated apoptosis in the hippocampus [13]–[15].

Building on its role in neurological disease, the cilium is known to play a role in memory formation. Aβ peptides have been observed binding the $G\alpha_i$ linked ciliary GPCR SSTR3 reducing cAMP levels and long-term potentiation (LTP), resulting in impaired novel

object recognition and spatial recall [16], [17]. Chemical and genetic manipulations of 5HTR6 in an Alzheimer's-like APP/PS1 mouse model modulates both ciliary length and cognitive ability [18]. Additionally, hippocampal ablation of IFT88, a transport protein necessary for cilia formation, impairs distant memory formation. Forebrain-specific IFT88 KO mice to struggle with novel object recognition, Morris water maze performance, and aversive fear conditioning, possibly through destabilization of perineuronal nets [19], [20].

One ciliary signaling protein that may give insight to how the cilium is linked to neural function is type 3 adenylyl cyclase (AC3). Originally identified in olfactory cilia, cAMP generated by AC3 is known to mediate the activation of CNG ion channels resulting in rapid depolarization of olfactory neurons [21]. Neuronal AC3 is not well studied outside of olfaction but it has become a protein of interest after human genome-wide association studies found a strong relation between AC3 and major depressive disorder (MDD) [22], [23]. AC3 is well known as a protein marker of the neuronal primary cilium. In mice ablation of AC3 reduces neuronal activity, and causes various depression-like phenotypes, including altered sleep patterns, similar to those seen in human patients [24].

While these findings indicate a link between primary cilia and memory formation, the use of behavioral paradigms presents its own set of challenges due to varying interpretations of test results, qualitative scoring, and behavioral variability. To examine if cilia regulate sleep and brainwave patterns in a quantitative manner we performed 24-hour continuous EEG/EMG recordings on inducible IFT88 knockout (KO) mice (IFT88 flox/flox UBC-Cre/ERT2, tamoxifen-inducible), permitting temporal ablation of primary cilia. Sleep patterns were recorded to compare if IFT88 KO mice have similarly altered sleep patterns as AC3 KO mice. Brain EEG waveform activity was analyzed to assess if cilia deletion alters basal neuronal activity. Cross-frequency-coupling (CFC) between theta and gamma frequency oscillations was calculated to better understand the cognitive impairments that have been seen in ciliary ablation models, since CFC is known to play a role in synaptic plasticity and consolidating short-term memory into long-term memory [25]–[29]. Our results show that temporal ablation of IFT88 alters sleep patterns, reduces EEG waveform

activity, and attenuates theta-gamma phase-amplitude coupling (PAC). These results support the notion that primary cilia are necessary for routine neural function, not only early development and cell division as was classically understood. Additionally, our results are set apart from other studies in the field by the use of quantitative EEG analysis of brain activity, power, and synchronization, rather than qualitative behavioral tests. This is also the first study to show that neuronal primary cilia influence PAC, which helps to elucidate the cilium's role in synaptic function and plasticity which underlie the formation and persistence of memory.

Results

Cilia ablation alters sleep bout patterns in inducible IFT88 KO mice.

Sleep disturbances including light sleep, shifts in sleep architecture, and increased rapid eye movement (REM) cycles are common phenotypes of major depressive disorder and have been observed in a transgenic AC3 knockdown mouse model for depression [24], [30]. To observe if IFT88 ablated mice have similar sleep phenotypes to AC3 ablated mice, 24-hour EEG/EMG recordings were acquired, manually scored, and analyzed for alterations in sleep patterning (**Figure 1**). On a percentage basis, inducible IFT88 KO mice spent comparable time awake, in restful non-REM sleep, or in REM sleep as their wild type littermates (**Figure 2A**). However, the average length of their non-REM sleep bouts and wake bouts increased significantly and almost doubled in length ($p=0.0454$ and $p=0.0179$) (**Figure 2B**). In addition, these mice were also significantly less likely to be aroused from sleep, showing an 82% decrease in arousals from deep non-REM sleep ($p=0.0024$) and an 86% decrease in arousals from REM sleep when in the light cycle (**Figure 2C**). These observations also carried over into the dark cycle, traditionally when mice spend much less time sleeping, with these mice also showing over an 80% decrease in arousals from deep sleep ($p=0.0459$).

Inducible IFT88 KO mice have reduced EEG waveform activity.

AC3 KO mice exhibit impaired neural activity, with a reduction in brain wave power similar to what has been observed in EEG recordings in human patients suffering from MDD [31], [32]. To characterize if IFT88 mice share this pathology the 24-hour EEG/EMG recordings were filtered to remove the DC offset as well as line current and then further processed in MATLAB to generate power spectrum density plots (PSDs; **Figure 3**). Inducible IFT88 KO mice had a broad reduction in brain power across the spectrum as well as a reduction in peak power during wake ($p=0.0171$) and non-REM ($p=0.0341$) mental states. More specifically, they lost approximately 47% of their power potential in the slow-wave delta-theta bands when in the awake state ($p=.0013$ for activity below 8Hz; **Figure 4**). When in non-REM and REM sleep the low wave power potential was not disrupted but instead there was a roughly 30% decrease in alpha and beta wave activity.

Cilia ablation leads to attenuation of theta-gamma phase-amplitude coupling.

It has been observed that different frequency bands of brain wave activity are not isolated and that their oscillations interact with each other through modulation (**Figure 5**). Multiple forms of this cross-frequency coupling (CFC) have been observed, however, phase-amplitude coupling (PAC) is the most studied form and is known to play a role in the integration of signals between different brain regions [33], [34]. In particular, slow-theta-to-gamma PAC in the human hippocampus has been found to support the formation of new episodic memories, and interactions between these bandwidths causes powerful and rapid action potential spiking leading to long-term potentiation at synapses [35], [36]. Slow-theta-to-gamma PAC has also been well documented to be reduced or disrupted in patients that suffer from neurological diseases such as Parkinson's disease, schizophrenia, and autism [37]–[39].

To quantify theta-gamma phase-amplitude coupling in IFT88 ablated mice, Canolty's mean-vector length modulation index (MVL-MI) method was initially used (**Figure 6**). This method estimates PAC from a signal of length N, by combining phase and amplitude

information to create a complex-valued signal: $f_a^{ei(\phi f_p)}$ for every time point. This generates a table of vectors and if the resulting probability distribution function is non-uniform, it suggests coupling between the phase frequency (f_p) and the amplitude frequency (f_a), which can be quantified by taking the length of the average vector [40]. First, for every individual experimental group PAC was calculated both with the pre-processed sample data and with a randomized version of the same dataset (to disrupt PAC) to calculate if PAC is present. Significant theta-high gamma PAC was only found to be occurring in the awake and non-REM states of WT mice when compared to their matching pseudo-dataset ($p<.0001$). The Modulation Index (MI) was then compared between groups using Tukey's HSD (note, a lower MI indicates stronger PAC). Using Canolty's MVL-MI we found that IFT88 deficient mice had impaired theta-gamma PAC both when awake ($p=0.0071$) and when in non-REM sleep ($p=0.0327$). This is evident by the reduced mean vector length in both of these signals ($p=0.0093$ and $p=0.0424$) as well a 90° shift in the phase angle across all states ($p=0.0366$, 0.0383, 0.0415).

It should be noted, however, that MI-values from the MVL-MI-Canolty algorithm have been shown to partly reflect the power of f_a oscillations, rather than the coupling strength between f_p and f_a. To further validate our conclusions, we applied a MI algorithm which includes a normalization factor that corresponds to the oscillatory power of f_a [37]. This method has also been seen to be more resilient to noise, which is preferential for EEG data that often has a lower signal to noise ratio than other electrophysiological recordings. Using this method, reductions in theta-gamma PAC strength during awake ($p<0.01$) and non-REM ($p<0.05$) activity were observed (**Figure 7**), consistent with our MVL-MI-Canolty based results. These findings suggest that the observed reduction in cross-frequency coupling is directly caused by the genetic ablation of the ciliary gene IFT88 and is not due to electrical noise or variance.

Discussion

Like AC3 KO depression model mice, inducible IFT88 KO mice were found to have altered sleep patterns, which is a common phenotype in human depression patients [24], [32]. The average sleep bout lengths of inducible IFT88 knockout mice were significantly longer than WT mice and they were aroused from sleep fewer times, indicating that inducible IFT88 KO mice are less likely to be stirred. This is possibly due to the state-dependent reductions in neural activity that were observed. Disrupted sleep patterns are also known to contribute to cognitive decline in Alzheimer's patients where they are believed to interfere with natural amyloid-β and tau clearing processes [41]–[43]

Inducible IFT88 KO mice had no changes in their high frequency gamma and beta bandwidths but had a reduction in slow rhythm theta and delta waves. Interestingly, while awake the brain is predominantly active at higher frequencies, indicating that inducible IFT88 KO mice have impaired ability to generate low frequency subconscious processes while awake. The inverse of this phenomenon was observed in sleep states. In both REM and non-REM states inducible IFT88 KO mice had reduced high frequency activity in the beta and alpha frequencies, but no changes in the slow frequency theta and delta waves which are the predominate bandwidths during rest.

To understand how these changes in sleep and brain activity could impact memory, EEG/EMG waveforms were analyzed for cross-frequency coupling (CFC). It was found that phase-amplitude coupling (PAC) between the theta and high-gamma frequencies was impaired in awake and in non-REM sleep of inducible IFT88 KO mice. PAC, specifically between the theta-gamma bandwidths, has a well-established role in memory formation and is known to be disrupted in humans afflicted with mild cognitive impairment, Alzheimer's, and Parkinson's [25], [44][45]. Based off these data we can postulate that inducible IFT88 KO mice will have impaired memory formation, which has been recorded in preliminary behavioral experiments [46].

Collectively this research indicates that ciliary function aids in brain wave propagation and synchronization which underlies the establishment and retention of memories. These characterizations of an inducible IFT88 KO mouse model are similar to what has been seen in AC3 KO mice, highlighting it as a complementary mouse model for the study of primary cilia in neurological function [24]. Our finding that cilia influence memory formation is consistent with what other groups have found, but our use of quantitative EEG and PAC analysis augments prior behavioral research [9]–[12], [15]–[18], [47]. This is also the first study to show that primary cilia influence PAC, providing a new level of insight into how genetic mutations influence the physical systems behind memory formation. This finding would have once been considered unlikely but our understanding of the primary cilium is constantly being redefined. Serial-section EM analysis has found that on average human cortical neuronal primary cilia form connections with the processes and cell bodies of 40-60 other cells. These intersections develop synapses, gap junctions, tight junctions, and other connections capable of propagating signals throughout the neural network [48]. Multiply these connections by the 86 billion neurons in the human brain and it is highly probable that the primary cilium influences a host of functions yet uncovered.

Further studies will need to be performed to understand which ciliary signaling pathways are contributing to brain wave power and PAC, but it is plausible that ciliary knock-out interferes with cAMP signaling within the cilium to produce these phenotypes. IFT88 is a subunit of the IFT-B complex responsible for anterograde transport and elongation of the cilium [49]. Ablation of this protein results in a lack of cilia formation and disrupts numerous signaling pathways including the ciliary GPCRs SSTR3 and 5-HTR6, both of which have been tied to cognition through genetic knock-out, pharmacological manipulation, and behavioral assays [16]–[18]. It will also perturb ciliary AC3 which has also been reported to influence contextual memory formation [50]. Adding further weight to the cAMP hypothesis are the findings that the primary cilium, despite its miniscule volume, is capable of generating cAMP signaling cascades independent of the cell body to influence adipogenesis and kidney cystogenesis [51], [52]. Previously this hypothesis would have been

difficult to prove due to the complexities of measuring cAMP in live-cells, but advancements in microscopy and the development of cilia specific cAMP biosensors will allow for further study of the primary cilium's role in memory and neural function [53].

Memory is one of the most advanced yet fundamental traits of intelligent life and when it is impaired by age or disease it can have devasting impacts on the individual and those close to them. Our experiments and the work from other research groups previously mentioned are providing a growing body of evidence that primary cilia are necessary for neural function and memory, not only in diseased patients but in healthy individuals. Our findings that primary cilia influence sleep, EEG waveforms, and PAC in inducible IFT88 KO mice will guide future research to elucidate the specific mechanisms that interlace memory and cognition with ciliary function.

Methods and materials

Animals and inducible ablation of IFT88 in mice.

All animal-related procedures were approved and conducted in accordance with the guidelines of the Institutional Animal Care and Use Committee of the University of New Hampshire. Mice were maintained on a 12-h light/dark cycle at 22°C and had access to food and water ad libitum. Mixed sex IFT88 flox/flox; UBC-Cre/ERT2 littermate mice of roughly two months of age were administered with tamoxifen dissolved in corn oil (0.2 mg/g body weight for consecutive 7 days), or corn oil as controls, via oral gavage to induce CRE recombinase expression. After the treatment course mice were allowed to rest for six weeks to allow for full genetic silencing and turn-over of IFT88. Mice were monitored after injection and for 24 hours after their last injection for any signs of discomfort. To prevent sexual bias, each genotype group had mixed sexes of mice.

EEG/EMG headmount Surgery

Surgery was performed as described previously (Chen et al. 2016 and Sterpka et al. 2020) and followed the manufacturer's instructions (Pinnacle Technology, Lawrence, Kansas). Briefly, Mice were anesthetized with an intraperitoneal injection of Ketamine (65mg/kg) /Xylazine (13mg/kg) cocktail and placed in a stereotaxic stage (Stoelting). The scalp was then opened along the sagittal plane and a three-pin EEG/EMG headmount (Pinnacle Technology) was implanted at the bregma. Mice were anesthetized with 1.5–2% isoflurane and secured in a stereotaxic device (Kopf Instruments). While under anesthesia, mice were prepared for surgery by hair removal, sterilization of skin with alcohol and 4% chlorhexidine. After exposing the skull surface, an EEG/EMG headmount (Pinnacle Technology Inc., Cat # 8201) was centered along the sagittal suture with the front edge 3.5 mm anterior to bregma, initially stabilized with VetBond. Headmount was then secured with four stainless steel screws (also functioned as EEG electrodes) and coated in acrylic for insulation. When positioned properly, all four screws (two anterior: AP 3.0 mm, ML ± 1.75 mm; two posterior: AP - 4.0 mm, ML ± 1.75 mm, relative to Bregma) sit on the cerebral region. Two EMG wires were inserted bilaterally into the trapezius muscles to monitor neck muscle activity. Skin was then sutured around the base of headmount. The headmount and surrounding screws and wires were then covered and sealed by dental cement.

EEG/EMG recording and sleep state scoring

EEG/EMG recording were performed as previously described (Chen et al. 2016 Biological Psyshiatry). Following surgery, the mice were given a week of recovery in their home cages before being individually tethered to EEG commutators within circular recording enclosures. They were then accustomed to the recording equipment in a free-moving state for two days. After acclimatization, continuous EEG/EMG signal collection was performed for a 24-hour period using Sirenia software from Pinnacle Technology (Lawrence, Kansas). The EEG/EMG signals underwent a 5,000-fold amplification and were sampled at 400 Hz. For classification into wakefulness, REM, and NREM sleep, EEG/EMG data were analyzed off-line. This process involved manual visual inspection supported by

the cluster scoring method of Sleep Pro Version 1.3 (Pinnacle Technology), leveraging standard criteria that consider signal amplitude, frequency, and regularity. In 10-second epochs, EEG/EMG sleep/wake events were initially scored as wake (characterized by low-amplitude, high-frequency EEG, and high-amplitude EMG), NREM sleep (marked by high-voltage, low-frequency EEG, and low-amplitude EMG), or REM sleep (exhibiting low-voltage EEG predominantly in theta waves and EMG atonia). After scoring, segments representing different sleep states were exported as separate .edf files for MATLAB analysis.

Signal preprocessing

Prior to analysis all signals were pre-processed in MATLAB R2020b using the open-source plugin Brainstorm v3 [54]. Because phase-amplitude coupling and density distributions are time dependent, all files of wake, non-REM, and REM data had to be standardized to a consistent time period. This was done by concatenating all individual files for a specific sleep state of an individual into one file and then trimming to a standard length. For awake data this was 15,000 seconds per animal, non-REM was 10,000 seconds per animal, and REM was 2,000 seconds per animal. After concatenation each file was band-pass filtered between 0.5 and 250 Hz (Butterworth filter, low-pass order 4, high-pass order 3) and band-stop filtered (59.5–60.5 Hz; 119.5–120.5 Hz) to remove 60 Hz power-line contamination and its harmonics.

Power spectrum densities

PSDs were calculated in Brainstorm using Welch's method with a 1 second window time and 25% overlap. Frequency bandwidths were delta 0.5-4Hz, theta 4-8Hz, alpha 8-13Hz, beta 13-30Hz, gamma 30 -200Hz. Significance was calculated using the Kolmogorov-Smirnov test.

Phase amplitude coupling (PAC)

PAC was calculated in the MATLAB plugin EEGLAB v2021.0 [55]. 3-10Hz was the phase frequency used for nesting against a high bandwidth of 50-120Hz. Modulation index was calculated using Canolty's mean-vector length modulation index method [40].

$$MI = \left|\frac{1}{N}\sum_{n-1}^{N} f_a(n)e^{i(\emptyset f_p(n))}\right|$$

Phase-sorted amplitude histograms were compared using the Kolmogorov-Smirnov test with a Bonferroni-Holm correction and a 95% confidence interval. Initially to test if theta-high gamma PAC was present each sample dataset was compared to a pseudo-dataset where the initial data was randomized to disrupt and negate any possible PAC that was occurring. PAC was also calculated in Brainstorm using a modified modulation index algorithm that contains a normalization factor to correct for oscillatory power [37].

$$MI = \frac{1}{\sqrt{N}} \frac{\left|\frac{1}{N}\sum_{n-1}^{N} f_a(n)e^{i(\emptyset f_p(n))}\right|}{\sqrt{\frac{1}{N}\sum_{n-1}^{N} f_a(n)^2}}$$

<u>Sample size and statistics</u>

Initial sample size was n = 8 control mice and n = 7 inducible IFT88 KO mice of mixed sex from similar litters. As noted above, due to corrupted files or mechanical failure the data from three wildtype and two KO mice were discarded reducing the sample size to n=5 wildtype and n = 5 inducible IFT88 knockout mice. Littermates were used in the experimental and control group to help reduce genetic variation and behavior between treatment groups. After acquisition labels were anonymized so the data could be scored blindly. Statistical comparisons were performed in JMP 15 Pro. First Shapiro-Wilk and Anderson-Darling goodness-of-fit tests were applied to evaluate normality of the data. Experiments with a normal distribution were compared using the Tukey-Kramer HSD while nonparametric results were compared using the Steel-Dwass test. For cumulative density plots of specific brain wave frequencies, the nonparametric Kolmogorov-Smirnov test was used to compare the distribution of brain wave activity.

Figures

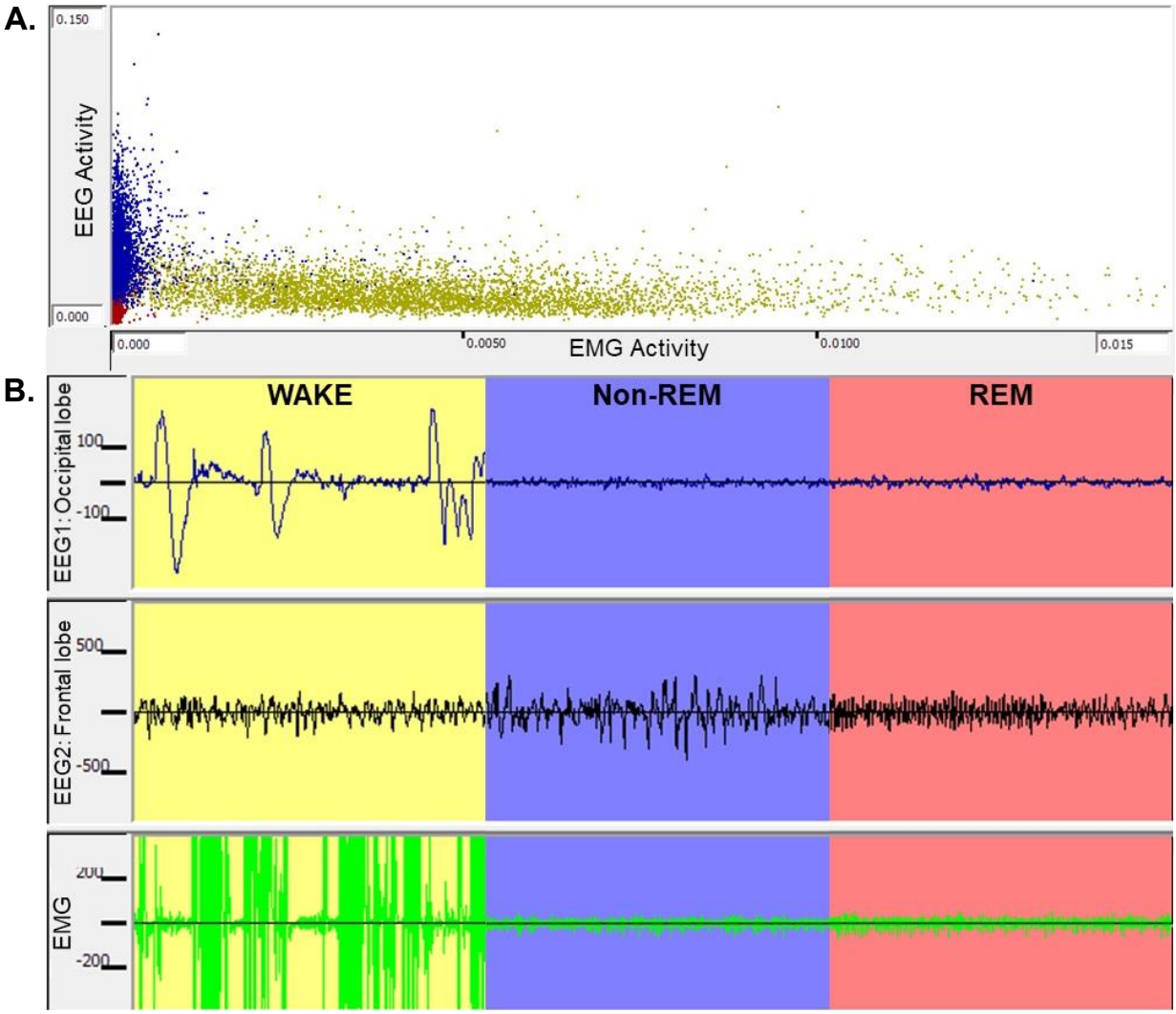

Figure 1: Manual scoring of mouse EEG/EMG electrophysiological recordings. **(A)** Example of how 24-hour recordings were scored in Sirenia Sleep 1.0.3 by comparing EEG to EMG signal strength to identify clusters of Wake, Non-REM, and REM data. **(B)** The recordings were manually curated in 10 second epochs to correct cluster scoring. The awake state is characterized by activity in the occipital lobe (EEG1), high frequency-low amplitude activity in the frontal lobe (EEG2), and high levels of EMG activity. Asleep mice lack EMG and occipital lobe activity. The non-REM state is identified by low frequency/high amplitude brain waveforms and REM sleep is differentiated by high frequency-low amplitude EEG activity, similar to what is seen while awake.

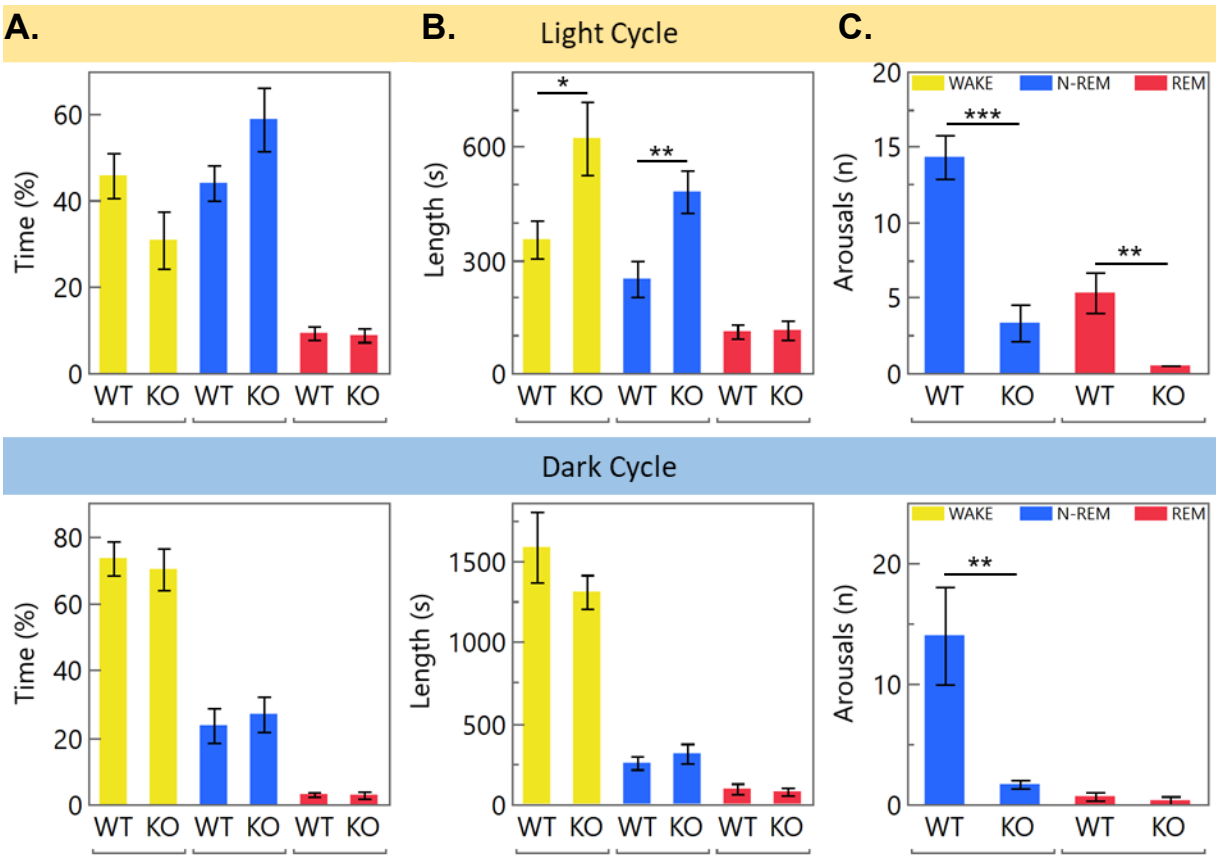

Figure 2: Sleep analysis of inducible IFT88 KO mice. **(A)** Ablation of primary cilia in inducible IFT88 KOs does not alter the light or dark cycle sleep patterns of mice **(B)** Average duration of wake and non-REM bouts was significantly increased (p=0.0454, 0.0179 respectively) in the light daytime cycle. **(C)** Inducible IF88KO mice were found to sleep more soundly than their WT littermates as they were aroused from non-REM (p=0.0024) and REM (p=0.0342) sleep far fewer times per sleep cycle than WT mice (Tukey's HSD test), n=5 WT and 5 KOs.

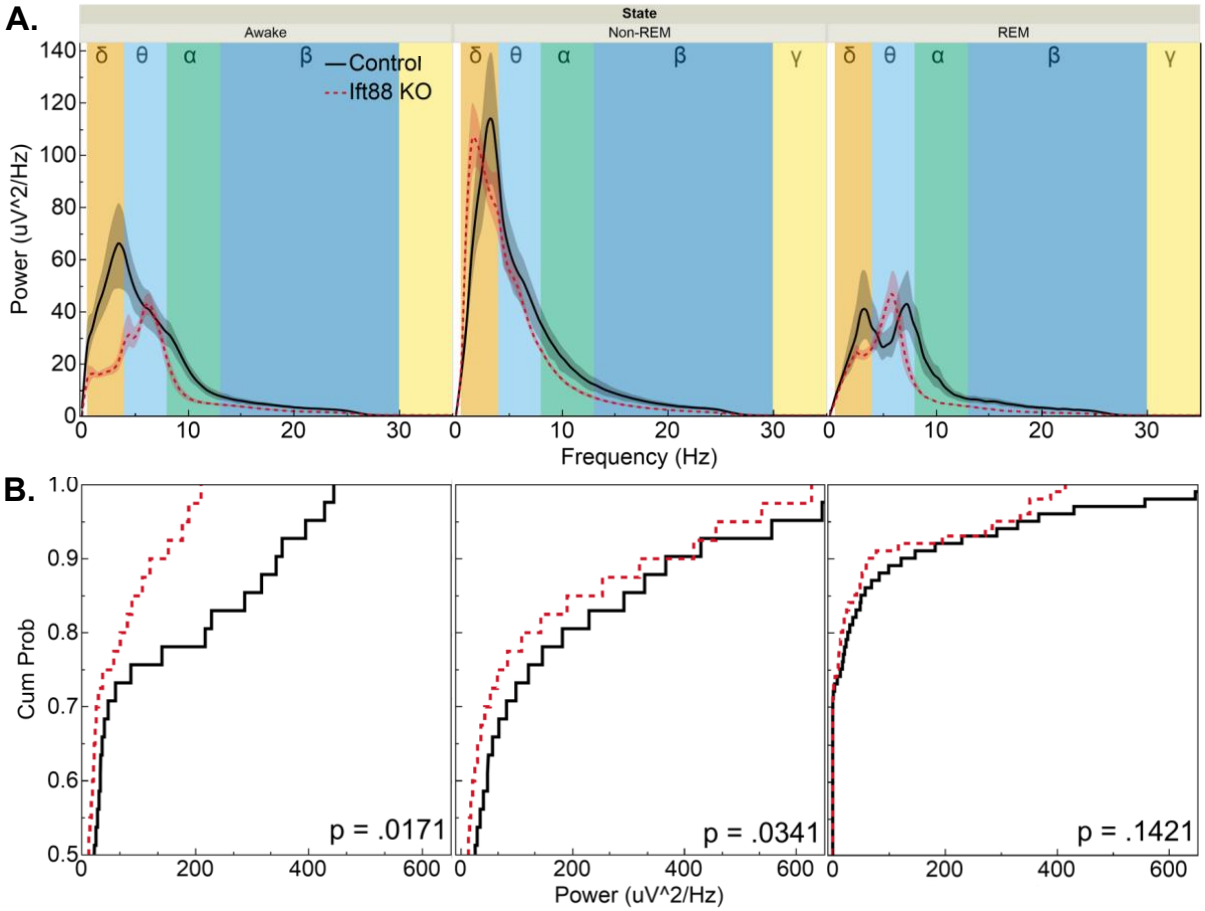

Figure 3: Inducible IFT88 KO mice have reduced EEG power over a broad spectrum. **(A)** Power spectrum density plots (PSDs) of EEG waveform power broken down by frequency ranges. Delta = 1 – 4 Hz, Theta = 4 – 8 Hz, Alpha = 8 – 13 Hz, Beta = 13 – 30 Hz, Gamma = 30 – 50 Hz. Overall EEG waveform activity was reduced in inducible IFT88 KOs in both the wake (p=0.0171) and non-REM (p=0.0341) states. **(B)** Cumulative distribution plots of **A** showing a general shift in EEG waveform to a lower power (Kolmogorov-Smirnov test).

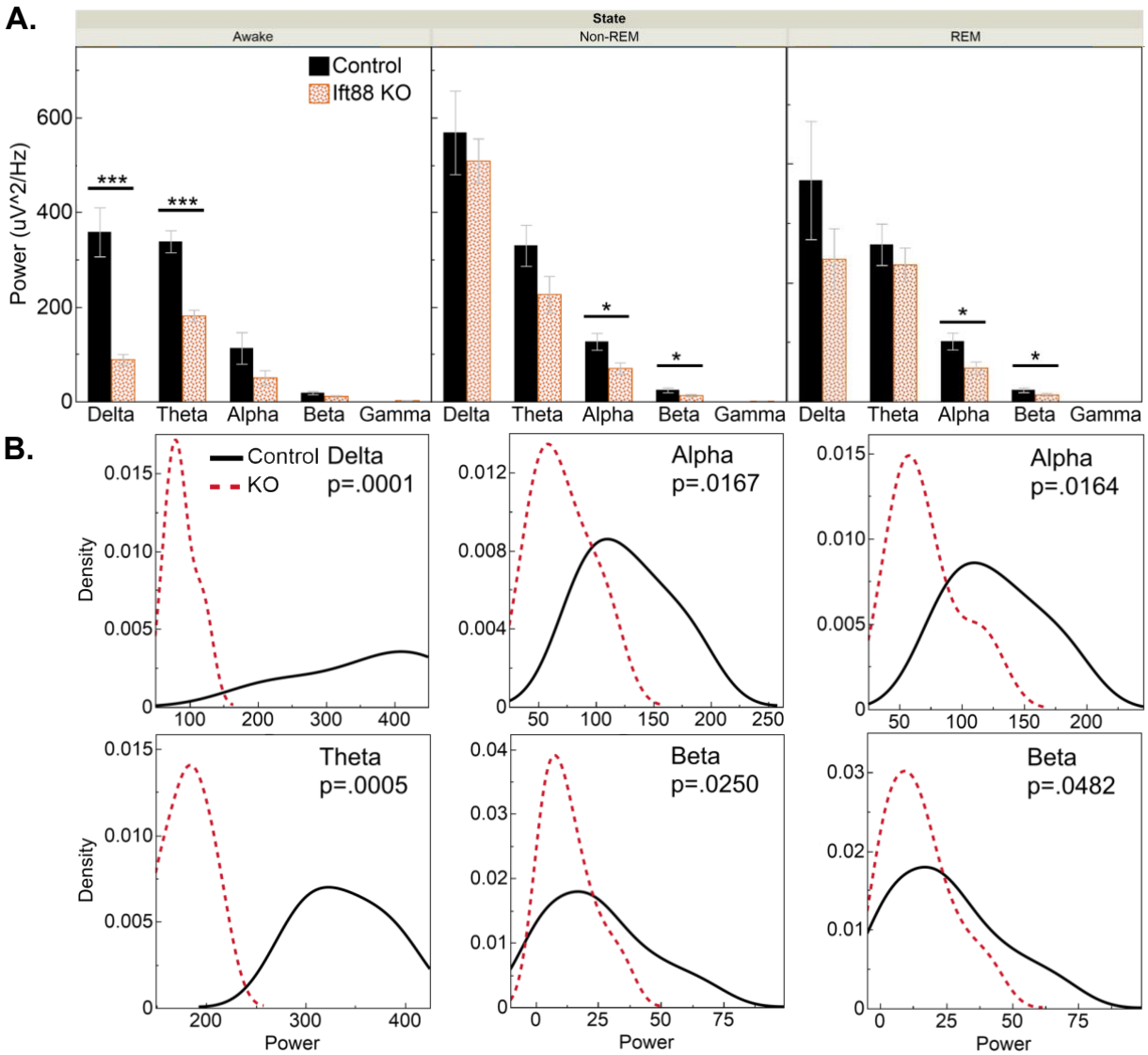

Figure 4: Ciliary ablation shifts EEG activity in a frequency dependent manner. **(A)** Decomposition of PSDs reveals that during the awake state, low-frequency delta wave activity was reduced by 75.1% (p=0.0059) and theta wave power was attenuated by 52.8% in inducible IFT88 KOs (p=0.0013). This response was sleep-state dependent as slow-wave power was not attenuated in Non-REM and REM sleep. During sleep states only power of high frequency waveforms was impacted. During non-REM sleep alpha and beta wave power was reduced by 44.2% (p=0.0167) and 45.9% (p=0.0265). This remained consistent in REM sleep where alpha wave power was attenuated 43.9% (p= 0.0179) and beta wave power by 40.65% (p=0.0492) (Tukey's HSD test). **(B)** Density distribution plots of this data illustrate how IFT88 ablation shifts peak brain power in these frequencies (Kolmogorov-Smirnov test).

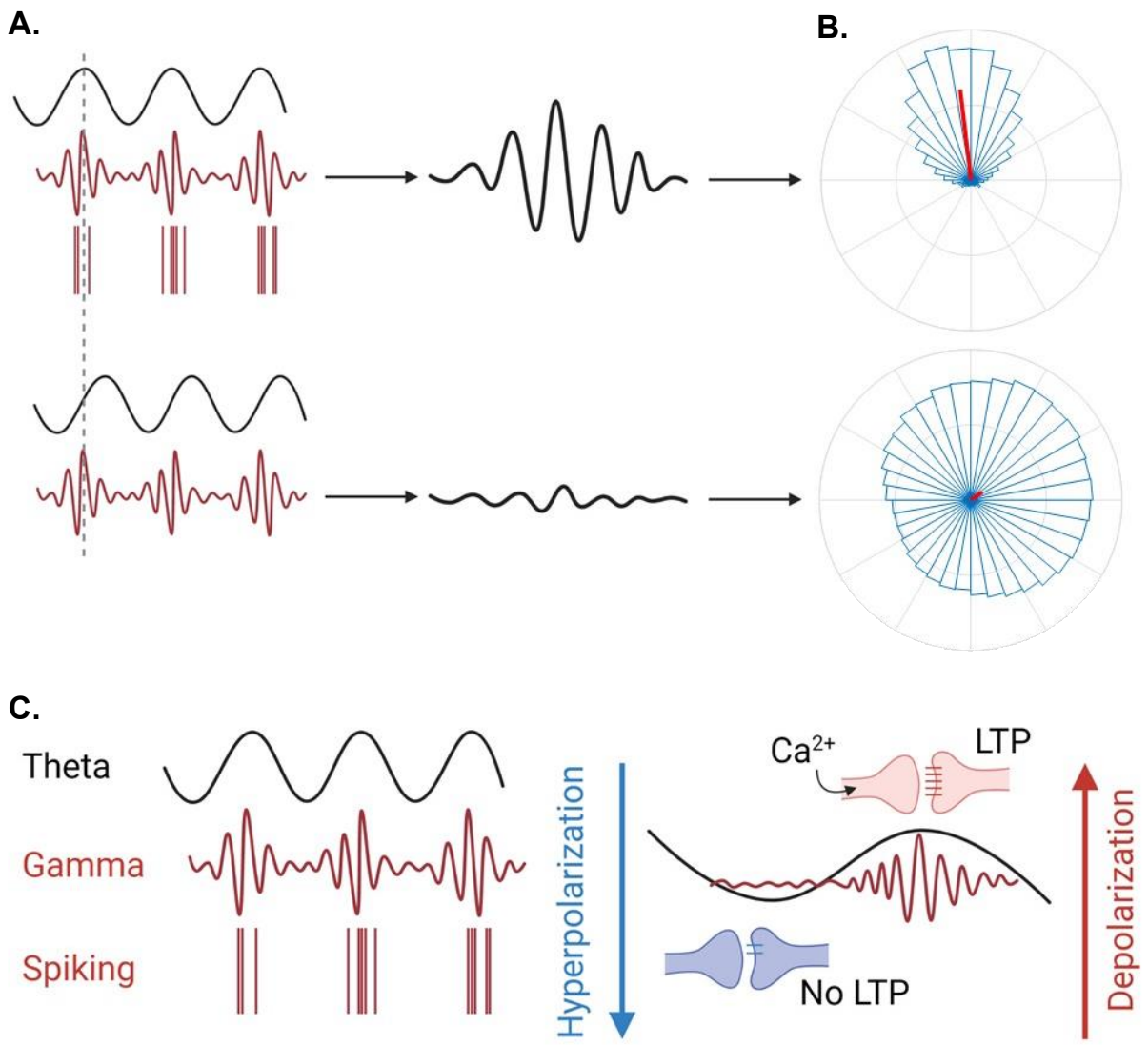

Figure 5: Phase-amplitude coupling. **(A)** When the phases of different frequency waveforms harmonize, PAC is characterized by the formation of harmonic Morlet wavelets. **(B)** In a polar histogram this can be quantified by a directional mean vector angle and mean vector length (red bar) which illustrates synchrony of the data set. When waveforms are not in phase they counteract each other, resulting in a lack of power and non-directional mean angle lengths and angles. **(C)** Synchronization of slow wave (4-8 Hz) and high wave (30-100 Hz) waveforms initiate an influx of Ca^{2+} to depolarize the cell and trigger fast action potential spiking. This spiking leads to strengthening of synaptic connections and promotion of Long-term potentiation.

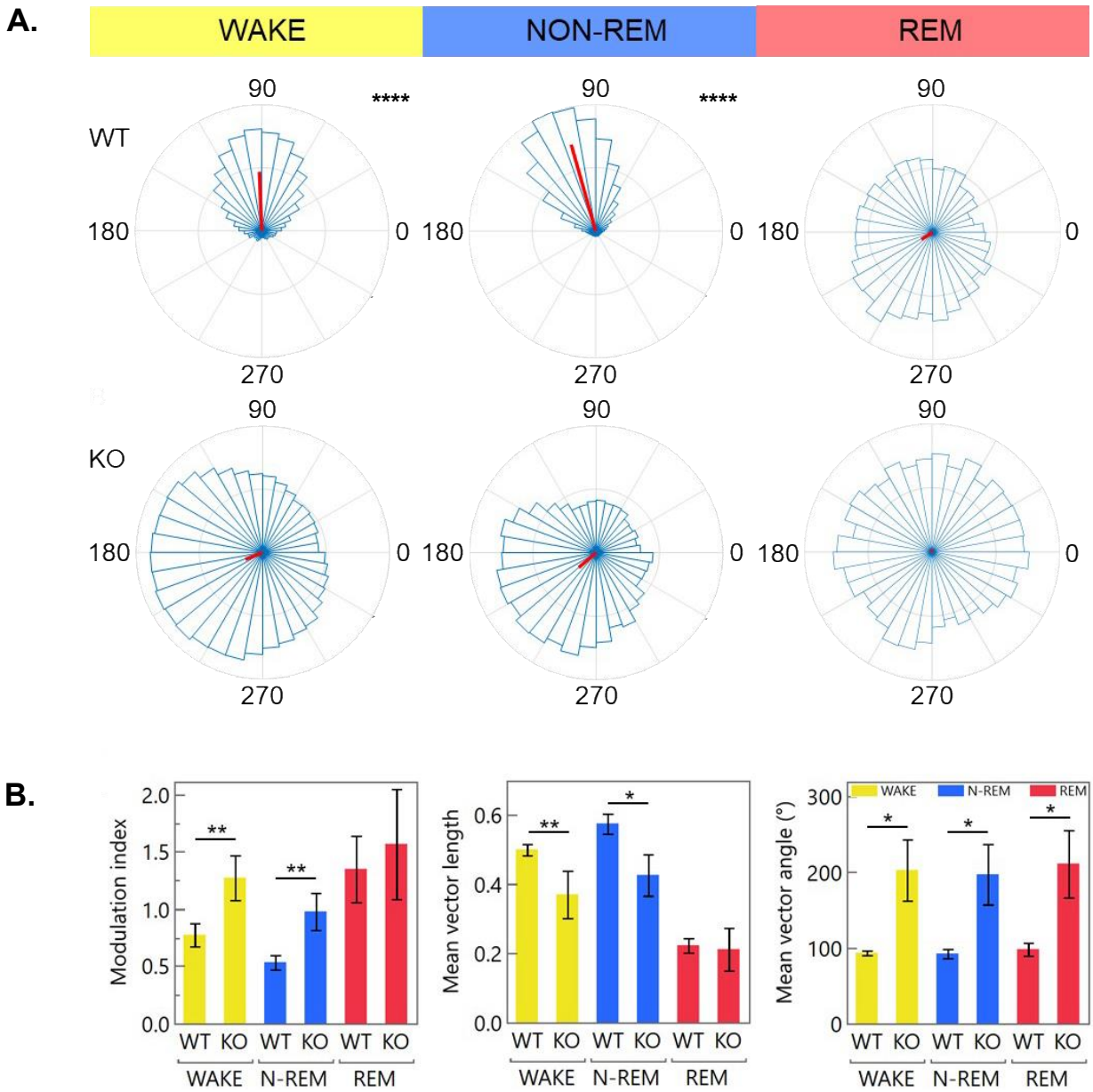

Figure 6: Inducible IFT88 KO mice have a reduced MVL-Canolty calculated PAC. **(A)** Representative polar histograms of modulation index vectors calculated using the MVL-MI-Canolty method shows the formation of theta-gamma phase-amplitude coupling only in WT mice during wake and non-REM states ($p<.0001$). This coupling is weak or not present in inducible IFT88 KO mice ($p>0.05$). **(B)** Using this algorithm a lower modulation index (MI) indicates stronger CFC. This reduction in PAC is quantified by a reduced mean vector length in wake ($p=0.0071$) and non-REM ($p=0.0032$) states as well as a 90° shift in their mean angle length vector in wake ($p=0.0366$), non-REM ($p=0.0383$), and REM ($p=0.0415$) states.

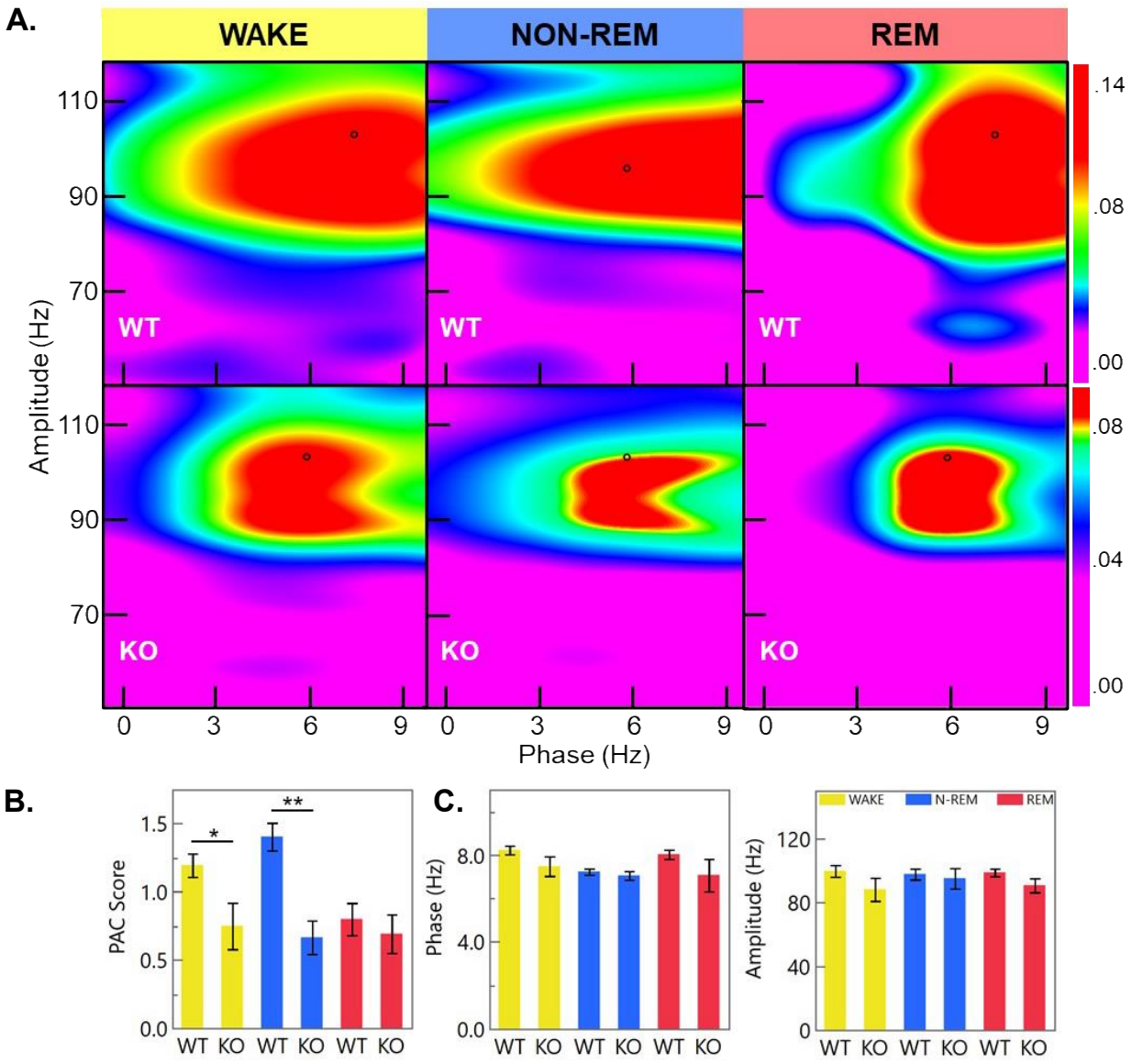

Figure 7: Theta-Gamma PAC is attenuated in inducible IFT88 KO mice. **(A)** Representative heatmaps show phase-amplitude coupling between the theta-high gamma frequencies calculated using an adjusted MVL algorithm. Black cursors represent peak PAC for each condition. **(B)** This algorithm corrects for oscillatory power in the signal used for PAC analysis to generate a PAC score value (a lower value indicates stronger PAC). Using this method inducible IFT88 KO mice still show a reduction in theta-high gamma cross frequency coupling during wake (p=0.0085) and non-REM (p=0.0372) states. **(C)** Cross phase coupling is highest at the intersection of 8 Hz and 101 Hz in WT mice; this is not significantly changed in inducible IFT88 KO mice indicating that PAC of KO mice is being attenuated and not shifted.

References

[1] S. C. Goetz and K. V. Anderson, “The primary cilium: A signalling centre during vertebrate development,” Nature Reviews Genetics, vol. 11, no. 5. Nature Publishing Group, pp. 331–344, May 2010, doi: 10.1038/nrg2774.

[2] A. Molla-Herman et al., “The ciliary pocket: An endocytic membrane domain at the base of primary and motile cilia,” J. Cell Sci., vol. 123, no. 10, pp. 1785–1795, May 2010, doi: 10.1242/jcs.059519.

[3] Y. C. Lin et al., “Chemically inducible diffusion trap at cilia reveals molecular sieve-like barrier,” Nat. Chem. Biol., vol. 9, no. 7, pp. 437–443, Jul. 2013, doi: 10.1038/nchembio.1252.

[4] F. R. Garcia-Gonzalo and J. F. Reiter, “Open Sesame: How transition fibers and the transition zone control ciliary composition,” Cold Spring Harb. Perspect. Biol., vol. 9, no. 2, 2017, doi: 10.1101/cshperspect.a028134.

[5] L. Schneider et al., “PDGFRαα signaling is regulated through the primary cilium in fibroblasts,” Curr. Biol., vol. 15, no. 20, pp. 1861–1866, Oct. 2005, doi: 10.1016/j.cub.2005.09.012.

[6] M. Simons et al., “Inversin, the gene product mutated in nephronophthisis type II, functions as a molecular switch between Wnt signaling pathways,” Nat. Genet., vol. 37, no. 5, pp. 537–543, May 2005, doi: 10.1038/ng1552.

[7] E. J. Ezratty, N. Stokes, S. Chai, A. S. Shah, S. E. Williams, and E. Fuchs, “A role for the primary cilium in notch signaling and epidermal differentiation during skin development,” Cell, vol. 145, no. 7, pp. 1129–1141, Jun. 2011, doi: 10.1016/j.cell.2011.05.030.

[8] J. F. Reiter and M. R. Leroux, “Genes and molecular pathways underpinning ciliopathies,” Nature Reviews Molecular Cell Biology, vol. 18, no. 9. Nature Publishing Group, pp. 533–547, Sep. 01, 2017, doi: 10.1038/nrm.2017.60.

[9] S. Ozonoff, B. J. Williams, S. Gale, and J. N. Miller, “Autism and Autistic Behavior in Joubert Syndrome:,” http://dx.doi.org/10.1177/088307389901401003, vol. 14, no. 10, pp. 636–641, Jul. 2016, doi: 10.1177/088307389901401003.

[10] Y. Luo et al., “Fragile X Mental Retardation Protein Regulates Proliferation and Differentiation of Adult Neural Stem/Progenitor Cells,” PLoS Genet., vol. 6, no. 4, Apr. 2010, doi: 10.1371/JOURNAL.PGEN.1000898.

[11] W. Guo et al., “Ablation of Fmrp in adult neural stem cells disrupts hippocampus-dependent learning,” Nat. Med. 2011 175, vol. 17, no. 5, pp. 559–565, Apr. 2011, doi: 10.1038/nm.2336.

[12] B. Lee, S. Panda, and H. Y. Lee, “Primary Ciliary Deficits in the Dentate Gyrus of

Fragile X Syndrome," Stem Cell Reports, vol. 15, no. 2, p. 454, Aug. 2020, doi: 10.1016/J.STEMCR.2020.07.001.

[13] S. X. Bamji et al., "The p75 Neurotrophin Receptor Mediates Neuronal Apoptosis and Is Essential for Naturally Occurring Sympathetic Neuron Death," J. Cell Biol., vol. 140, no. 4, p. 911, Feb. 1998, doi: 10.1083/JCB.140.4.911.

[14] B. Chakravarthy et al., "The p75 neurotrophin receptor is localized to primary cilia in adult murine hippocampal dentate gyrus granule cells," Biochem. Biophys. Res. Commun., vol. 401, no. 3, pp. 458–462, Oct. 2010, doi: 10.1016/J.BBRC.2010.09.081.

[15] K. Tanaka, C. E. Kelly, K. Y. Goh, K. B. Lim, and C. F. Ibáñez, "Death Domain Signaling by Disulfide-Linked Dimers of the p75 Neurotrophin Receptor Mediates Neuronal Death in the CNS," J. Neurosci., vol. 36, no. 20, p. 5587, May 2016, doi: 10.1523/JNEUROSCI.4536-15.2016.

[16] E. B. Einstein et al., "Somatostatin Signaling in Neuronal Cilia Is Criticalfor Object Recognition Memory," J. Neurosci., vol. 30, no. 12, p. 4306, Mar. 2010, doi: 10.1523/JNEUROSCI.5295-09.2010.

[17] M. Solarski, H. Wang, H. Wille, and G. Schmitt-Ulms, "Somatostatin in Alzheimer's disease: A new Role for an Old Player," Prion, vol. 12, no. 1, p. 1, Jan. 2018, doi: 10.1080/19336896.2017.1405207.

[18] L. Hu, B. Wang, and Y. Zhang, "Serotonin 5-HT6 receptors affect cognition in a mouse model of Alzheimer's disease by regulating cilia function," Alzheimer's Res. Ther. 2017 91, vol. 9, no. 1, pp. 1–17, Sep. 2017, doi: 10.1186/S13195-017-0304-4.

[19] N. F. Berbari et al., "Hippocampal and cortical primary cilia are required for aversive memory in mice," PLoS One, vol. 9, no. 9, Sep. 2014, doi: 10.1371/journal.pone.0106576.

[20] V. Jovasevic, H. Zhang, A. Fischer, and R. Jelena, "iScience ll Primary cilia are required for the persistence of memory and stabilization of perineuronal nets," ISCIENCE, vol. 24, no. 6, p. 102617, 2021, doi: 10.1016/j.isci.2021.102617.

[21] W. ST et al., "Disruption of the type III adenylyl cyclase gene leads to peripheral and behavioral anosmia in transgenic mice," Neuron, vol. 27, no. 3, pp. 487–497, 2000, doi: 10.1016/S0896-6273(00)00060-X.

[22] W. NR et al., "Genome-wide association study of major depressive disorder: new results, meta-analysis, and lessons learned," Mol. Psychiatry, vol. 17, no. 1, pp. 36–48, Jan. 2012, doi: 10.1038/MP.2010.109.

[23] D. L. Cousminer et al., "Genome-wide association and longitudinal analyses reveal genetic loci linking pubertal height growth, pubertal timing and childhood adiposity," Hum. Mol. Genet., vol. 22, no. 13, p. 2735, Jul. 2013, doi: 10.1093/HMG/DDT104.

[24] X. Chen et al., “Ablation of Type III Adenylyl Cyclase in Mice Causes Reduced Neuronal Activity, Altered Sleep Pattern, and Depression-Like Phenotypes,” Biol. Psychiatry, vol. 80, no. 11, p. 836, Dec. 2016, doi: 10.1016/J.BIOPSYCH.2015.12.012.

[25] J. E. Lisman and O. Jensen, “The Theta-Gamma Neural Code,” Neuron, vol. 77, no. 6, p. 1002, Mar. 2013, doi: 10.1016/J.NEURON.2013.03.007.

[26] T. O. Bergmann and J. Born, “Phase-Amplitude Coupling: A General Mechanism for Memory Processing and Synaptic Plasticity?,” Neuron, vol. 97, no. 1, pp. 10–13, Jan. 2018, doi: 10.1016/J.NEURON.2017.12.023.

[27] C. Mikutta et al., “Phase-amplitude coupling of sleep slow oscillatory and spindle activity correlates with overnight memory consolidation,” J. Sleep Res., vol. 28, no. 6, 2019.

[28] M. Abubaker, “Working Memory and Cross-Frequency Coupling of Neuronal Oscillations,” vol. 12, no. October, pp. 1–14, 2021, doi: 10.3389/fpsyg.2021.756661.

[29] O. Papaioannou et al., “brain sciences Is Cortical Theta-Gamma Phase-Amplitude Coupling,” 2022.

[30] P. L, B. C, C. A, G. A, and R. D, “REM sleep dysregulation in depression: state of the art,” Sleep Med. Rev., vol. 17, no. 5, pp. 377–390, Oct. 2013, doi: 10.1016/J.SMRV.2012.11.001.

[31] A. Y. Shestyuk, P. J. Deldin, J. E. Brand, and C. M. Deveney, “Reduced Sustained Brain Activity During Processing of Positive Emotional Stimuli in Major Depression,” Biol. Psychiatry, vol. 57, no. 10, pp. 1089–1096, May 2005, doi: 10.1016/J.BIOPSYCH.2005.02.013.

[32] Y. Zhang et al., “Identification of psychiatric disorder subtypes from functional connectivity patterns in resting-state electroencephalography,” Nat. Biomed. Eng., vol. 5, no. April, 2021, doi: 10.1038/s41551-020-00614-8.

[33] S. Vanhatalo, J. M. Palva, M. D. Holmes, J. W. Miller, J. Voipio, and K. Kaila, “Infraslow oscillations modulate excitability and interictal epileptic activity in the human cortex during sleep,” Proc. Natl. Acad. Sci., vol. 101, no. 14, pp. 5053–5057, Apr. 2004, doi: 10.1073/PNAS.0305375101.

[34] R. T. Canolty and R. T. Knight, “The functional role of cross-frequency coupling,” Trends Cogn. Sci., vol. 14, no. 11, pp. 506–515, Nov. 2010, doi: 10.1016/J.TICS.2010.09.001.

[35] M. L. Schölvinck, D. A. Leopold, M. J. Brookes, and P. H. Khader, “The contribution of electrophysiology to functional connectivity mapping,” Neuroimage, vol. 80, pp. 297–306, Oct. 2013, doi: 10.1016/J.NEUROIMAGE.2013.04.010.

[36] P. Tewarie et al., “Functional brain networks: Linking thalamic atrophy to clinical

disability in multiple sclerosis, a multimodal fMRI and MEG Study," Hum. Brain Mapp., vol. 36, no. 2, pp. 603–618, Feb. 2015, doi: 10.1002/HBM.22650.

[37] T. E. Özkurt and A. Schnitzler, "A critical note on the definition of phase–amplitude cross-frequency coupling," J. Neurosci. Methods, vol. 201, no. 2, pp. 438–443, Oct. 2011, doi: 10.1016/J.JNEUMETH.2011.08.014.

[38] K. Kirihara, A. J. Rissling, N. R. Swerdlow, D. L. Braff, and G. A. Light, "Hierarchical Organization of Gamma and Theta Oscillatory Dynamics in Schizophrenia," Biol. Psychiatry, vol. 71, no. 10, pp. 873–880, May 2012, doi: 10.1016/J.BIOPSYCH.2012.01.016.

[39] K. Kessler, R. A. Seymour, and G. Rippon, "Brain oscillations and connectivity in autism spectrum disorders (ASD): new approaches to methodology, measurement and modelling," Neurosci. Biobehav. Rev., vol. 71, pp. 601–620, Dec. 2016, doi: 10.1016/J.NEUBIOREV.2016.10.002.

[40] R. T. Canolty et al., "High Gamma Power Is Phase-Locked to Theta Oscillations in Human Neocortex," Science, vol. 313, no. 5793, p. 1626, Sep. 2006, doi: 10.1126/SCIENCE.1128115.

[41] K. R. Sewell, K. I. Erickson, S. R. Rainey-Smith, J. J. Peiffer, H. R. Sohrabi, and B. M. Brown, "Relationships between physical activity, sleep and cognitive function: A narrative review," Neurosci. Biobehav. Rev., vol. 130, no. March, pp. 369–378, 2021, doi: 10.1016/j.neubiorev.2021.09.003.

[42] L. Peter-Derex, P. Yammine, H. Bastuji, and B. Croisile, "Sleep and Alzheimer's disease," Sleep Med. Rev., vol. 19, pp. 29–38, 2015, doi: 10.1016/j.smrv.2014.03.007.

[43] L. HY et al., "Bidirectional regulation of dendritic voltage-gated potassium channels by the fragile X mental retardation protein," Neuron, vol. 72, no. 4, pp. 630–642, Nov. 2011, doi: 10.1016/J.NEURON.2011.09.033.

[44] M. S. Goodman et al., "Theta-Gamma Coupling and Working Memory in Alzheimer's Dementia and Mild Cognitive Impairment," Front. Aging Neurosci., vol. 0, no. APR, p. 101, Apr. 2018, doi: 10.3389/FNAGI.2018.00101.

[45] R. Gong et al., "Cross-frequency phase-amplitude coupling in repetitive movements in patients with Parkinson's disease," J. Neurophysiol., vol. 127, no. 6, pp. 1606–1621, 2022, doi: 10.1152/jn.00541.2021.

[46] Y. Zhou, L. Qiu, M. Lyon, and X. Chen, "Activity Hierarchy Measurement to Establish Trace Memory-eligible 'Primed' Neurons," bioRxiv, 2023, doi: 10.1101/2023.01.06.523038.

[47] B. Chakravarthy, C. Gaudet, M. Michel, and J. Whitfield, "Amyloid- β Peptides Stimulate the Expression of the p75 NTR Neurotrophin Receptor in SH-SY5Y Human Neuroblastoma Cells and," vol. 19, pp. 915–925, 2010, doi: 10.3233/JAD-2010-1288.

[48] J. Y. Wu et al., “Mapping of neuronal and glial primary cilia contactome and connectome in the human cerebral cortex,” Neuron, pp. 1–15, 2023, doi: 10.1016/j.neuron.2023.09.032.

[49] T. Kobayashi, Y. Ishida, T. Hirano, Y. Katoh, and K. Nakayama, “Cooperation of the IFT-A complex with the IFT-B complex is required for ciliary retrograde protein trafficking and GPCR import,” Mol. Biol. Cell, vol. 32, no. 1, pp. 45–56, 2021, doi: 10.1091/MBC.E20-08-0556.

[50] Z. Wang, T. Phan, and D. R. Storm, “The type 3 adenylyl cyclase is required for novel object learning and extinction of contextual memory: Role of camp signaling in primary cilia,” J. Neurosci., vol. 31, no. 15, pp. 5557–5561, Apr. 2011, doi: 10.1523/JNEUROSCI.6561-10.2011.

[51] J. N. Hansen et al., “A cAMP signalosome in primary cilia drives gene expression and kidney cyst formation,” EMBO Rep., vol. 23, no. 8, Aug. 2022, doi: 10.15252/embr.202154315.

[52] K. I. Hilgendorf et al., “Omega-3 Fatty Acids Activate Ciliary FFAR4 to Control Adipogenesis,” Cell, vol. 179, no. 6, pp. 1289-1305.e21, 2019, doi: 10.1016/j.cell.2019.11.005.

[53] J. Y. Jiang, J. L. Falcone, S. Curci, and A. M. Hofer, “Direct visualization of cAMP signaling in primary cilia reveals up-regulation of ciliary GPCR activity following Hedgehog activation,” Proc. Natl. Acad. Sci. U. S. A., vol. 116, no. 24, pp. 12066–12071, 2019, doi: 10.1073/pnas.1819730116.

[54] F. Tadel, S. Baillet, J. C. Mosher, D. Pantazis, and R. M. Leahy, “Brainstorm: A user-friendly application for MEG/EEG analysis,” Comput. Intell. Neurosci., vol. 2011, 2011, doi: 10.1155/2011/879716.

[55] D. A and M. S, “EEGLAB: an open source toolbox for analysis of single-trial EEG dynamics including independent component analysis,” J. Neurosci. Methods, vol. 134, no. 1, pp. 9–21, Mar. 2004, doi: 10.1016/J.JNEUMETH.2003.10.009.